2.5-Bit/Detected Photon Demonstration Program: Description, Analysis, and Phase I Results

J. R. Lesh, J. Katz, H. H. Tan, and D. Zwillinger
Communications System Research Section

An optical communications demonstration program designed to demonstrate 2.5 bits of information transfer per single detected photon is described. The program was divided into four demonstration phases representing increasing degrees of complexity. The theoretical analysis of each of the phases is presented where it is shown that the 2.5-bit/detected photon goal can be achieved. The experimental results of phase I, which are in excellent agreement with the theory, are also presented,

I. Introduction

As deep space missions reach to greater distances and the scientific objectives of such missions become more ambitious the requirements for greater communication capability will continue to challenge the communications engineer. Past challenges have resulted in the transition from the S-band to the X-band frequency range, the increase in spacecraft antenna size and the arraying of multiple ground receive stations. Indeed the physical appearance of the Voyager-class spacecraft is completely dominated by the high-gain communications antenna. One cannot help wondering how much further such dimensions can be extended before reaching the limits of practicality.

One solution to this dilemma is to utilize optical frequencies for communications (Ref. 1). At optical frequencies the aperture determining components are usually measured in centimeters rather than meters. Furthermore, with the emergence of semiconductor injection lasers, one can reasonably anticipate that rugged, efficient solid-state optical sources will be available in the near future (Ref. 2). But even more significant is the fact that for receivers employing direct photon detection the communications channel capacity is extremely large, with only a moderate amount of optical signal energy. This point was discussed by Pierce in 1978 (Ref. 3) where he described a channel capable of conveying tens of bits of information for each signal photon. This might seem quite surprising since the classical (nonquantum) theory predicted a limit of only one nat of information per photon (1 nat = 1.44 bits). However, Pierce was really illuminating and expanding upon predictions that had been made some time earlier (Refs. 4-7) and which have now stood the test of time.

Although channel capacity is recognized as the ultimate throughput limit of the channel, it leaves unanswered the question of how one can approach that limit in practice. For this reason a number of studies were initiated to find good modulation and coding schemes for the optical channel. It is now known that by properly matching these two areas, transmission of up to 5 bits/photon is achievable with today's technology (Refs. 8, 9). All of these schemes employ M-ary pulse position modulation and either Reed-Solomon codes or interleaved, short-constraint-length (multiple) convolutional codes. Furthermore, achieving energy efficiencies greater than 5 bits/photon is impeded only by the present-day limits of signal processing complexity, limits which are rapidly receding with the onslaught of VLSI technology.

Thus far only theoretical performance calculations have been carried out. The results of such calculations depend very heavily on the validity of the mathematical models used to describe the system. For this reason a demonstration program was initiated to prove out the validity of the models and with the prime objective of demonstrating reliable communications at a data rate of at least 100 kbps and an energy efficiency of 2.5 bits/detected photon. (Reliable communications was defined as the Voyager threshold bit error rate of 5×10^{-3}.) The 2.5-bit/photon number was selected because it is comfortably above the classical limit but sufficiently small so that the system complexity would not get out of hand. After flushing out the problems at this design point a more ambitious program to demonstrate 5 or more bits/detected photon will be initiated.

In the next section we will describe the 2.5-bit/detected photon demonstration program and show how it has been divided into four program phases. In Section III we will present a theoretical analysis of the system and show that the primary demonstration goal can theoretically be achieved. This analysis is substantially more detailed than previous studies which tended to ignore such things as photomultiplier tube gain dispersion and thermal noise in the predetection pulse amplifier. In Section IV we will then describe the experimental results of the first phase of the program which show that the detector noise models used in the analysis are comfortably close to reality. Finally, the results are summarized and discussed in Section V.

II. General Description of the 2.5 Bit/Detected Photon Program

A block diagram of the demonstration system is shown in Fig. 1. The heart of the optical portion of the system consists of a gallium arsenide semiconductor injection laser and a direct detection photomultiplier tube. The GaAs laser diode is a high-quality, single-spatial-mode device operating at 0.85 μm and has the reliability and durability characteristic of solid-state devices. The light emitted from the laser is passed through some elementary optics followed by 70-100 dB of neutral density filters (attenuators) which simulate space loss. The attenuated optical signal is then applied to a photomultiplier tube (PMT) detector which has a high internal gain ($>10^6$), a quantum efficiency around 20% and, with moderate cooling, an extremely low dark current. Of course, to eliminate stray laboratory light, all of the optical components must be placed in an extremely dark enclosure.

Surrounding the optical components are the modulation and coding hardware. The laser diode is driven by a 256-slot/word PPM modulator which decides, based on an 8-bit input word, which slot the pulse should be placed in and then provides a current pulse during that slot to turn on the laser. Obviously, the inverse of this process is applied to the PMT output to recreate the 8-bit word. To improve the performance of the system, an 8-bit Reed-Solomon code is then used to surround the PPM portion of the system. An 8-bit Reed-Solomon encoder considers 8-bit segments of the incoming (binary) data stream as individual (generalized) symbols and then performs error correction coding over the strings of these generalized symbols. Since the code symbol size and PPM word size are matched, PPM word erasures or errors correspond to a single Reed-Solomon code symbol erasures or errors respectively. Such codes are well known for their burst erasure fill-in capabilities and, furthermore, can compensate for combinations of errors and erasures. The data streams supplied to the encoder and delivered from the decoder are then compared for an overall bit error rate measurement.

The demonstration program has been divided into four phases. The first phase involves only the PMT and its associated preamplifier and is intended to characterize the dark current noise distribution of the detection system. This phase has essentially been completed and the results will be described in Section IV. In the second phase (currently in progress) the laser will be added and the optical pulse erasure and error statistics will be evaluated. The PPM modulator and demodulator, which have already been designed and fabricated, will be added in phase III so that the PPM word error and word erasure probabilities can be measured. The final phase will encompass the coding hardware and will demonstrate the 2.5-bit performance goal.

III. Theoretical Analysis of the Demonstration

In this section we will analyze the performance of the 2.5-bit/detected photon demonstration system. A theoretical model of a photomultiplier tube and associated preamplifier was developed in Ref. 10. This model includes the effects of the photomultiplier tube random gain as well as post PMT preamplifier noise and is useful for computing communication system error performance as well as estimating, from experimental data, system parameters such as the PMT dark current. We will first describe the results in Ref. 10 pertaining to the model of the PMT gain random variable and the calculation of its probability density function. Then, using this model we will determine the detection and false alarm probabilities of a photocathode electron emission event. These results will be useful in characterizing both the dark current photoelectron emission event statistics (phase I) as well as optical pulse detection statistics (phase II). Next the pulse detection statistics are used to evaluate the error performance of the PPM

(uncoded) signal set. Finally, the coded PPM performance will be analyzed.

A. Random Photomultiplier Tube Gain

In a photomultiplier tube, electrons emitted by the photocathode (either from dark current or photon absorption) are directed through a series of dynodes by an electric field. Secondary electrons are emitted at each dynode for each impinging primary electron. The number of secondary electrons at each dynode is a random quantity and results in a random overall gain for the PMT. The mean and variance of this gain can be readily derived. An explicit expression for the exact probability distribution of the gain, however, is not available and the problem of determining it appears to be intractable. Since an analytical expression for this distribution is required to determine communication system error performance, a good approximation of the exact distribution is useful. In Ref. 10, such an approximation was derived by using a diffusion model. The approximate density $p_G(x)$ of the random gain G is given by

$$P_G(x) = e^{-\overline{G}/B}\left\{\delta(x) + \left(\frac{1}{B}\sqrt{\frac{\overline{G}}{x}}\right) e^{-x/B} I_1\left(2\,\frac{1}{B}\sqrt{\overline{G}\,x}\right)\right\}, \tag{1}$$

where $\delta(x)$ is the unit impulse function, $I_1(\cdot)$ is the modified Bessel function of the first kind,

$\overline{G}$ = average gain of the photomultiplier tube

ν = number of dynode stages

and where the parameter B is specified by $\overline{G}$ and ν according to

$$B = \frac{1}{2}\,\frac{\overline{G} - 1}{\sqrt[\nu]{\overline{G}} - 1}. \tag{2}$$

This approximate density yields the correct mean and variance for G. In fact, the variance of G is simply given by $2\overline{G}B$. For the RCA C31034 PMT used in this demonstration $\overline{G}$ is about 10^6 and $\nu = 11$, so the standard deviation of G is about $0.6\overline{G}$ and B is equal to about one-third of the standard deviation. Figures 2(a) and 2(b) plot the density of the normalized gain $G/\overline{G}$ as given by (1) for the PMT used in the demonstration at $\overline{G} = 10^6$ and 10^7 respectively. As can be seen from these figures, the density is not symmetric about the mean and has substantial probability mass in the region below its mean value $\overline{G}$. This means that there is substantial likelihood that the photomultiplier output signal level will be lower than the corresponding average gain value, and error performance calculations based on a constant gain model will not be accurate. Also shown in Fig. 2 is a density function that is the positive truncation of the Gaussian density having the same mean and variance as $p_G(x)$. It is clear that using the simpler Gaussian approximation can produce results that are substantially optimistic.

B. Photocathode Emission Event Detection: Receiver Operating Curves

In phase I of the demonstration the number of dark current emission events at the PMT cathode is experimentally recorded by monitoring the PMT output with a pulse counter. In Ref. 10, the effects of random PMT gain, thermal noise in the post PMT preamplifier, and counter response time on successful photocathode dark current emission event detection were evaluated. The PMT anode output is assumed to be terminated by a resistor of R ohms. The voltage signal $S(t)$ across this resistor is amplified and fed into a pulse counter. The amplifier-counter combination is modeled as an additive thermal noise $V(t)$ followed by a short term time averager over T_c seconds (the counter response time). The output of this time averager is then compared with a threshold γ. An emission event is recorded by the counter only when the threshold γ is exceeded. The entire system is shown in Fig. 3. The additive thermal noise $V(t)$ is assumed to have spectral density

$$N_0 = k\theta R \text{ (volts)}^2/\text{Hz} \tag{3}$$

where k = Boltzmann's constant, θ = noise equivalent temperature of the amplifier and R = amplifier equivalent resistance (assumed to be matched to the anode terminating resistance). If P_d = detection probability of an emission event and P_f = false alarm probability due to thermal noise, then it is shown in Ref. 10 that

$$P_d = \int_0^\infty Q\left(\frac{\gamma - \left(\frac{eR}{T_c}\right)x}{\sigma}\right) P_G(x)\,dx, \tag{4}$$

and

$$P_f = Q\left(\frac{\gamma}{\sigma}\right), \tag{5}$$

where $p_G(x)$ is given by (1) and where

$$Q(\chi) = \int_\chi^\infty \frac{1}{\sqrt{2\pi}}\, e^{-t^2/2}\,dt,$$

and

$$\sigma^2 = \frac{N_0}{T_c} .$$

Receiver operating curves of P_d versus P_f are shown in Fig. 4 for a counter response time T_c = 10 ns, thermal noise standard deviation σ = 34 μV and for several values of PMT average gain $\overline{G}$. Also shown on the figure are the corresponding threshold values.

These curves are useful in interpreting pulse counter data for the purpose of determining whether the number of dark current photoelectrons is Poisson distributed. Suppose pulse counter data is recorded over a period of 1 sec and the counter response time T_c = 10 nsec. Assume that the average gain of the photomultiplier $\overline{G} = 10^6$ and the PMT is cooled to -30°C. With these parameters the RCA C31034 PMT is rated to have an average dark current emission rate at the photocathode of about 25 counts per second. Then under an assumption of Poisson statistics, the probability of one dark current photoelectron emission event in an interval of T_c = 10 nsec is about

$$\lambda_n = 25\, T_c = 2.5 \times 10^{-7}$$

and the probability of no dark current events is approximately $1 - \lambda_n$. The probability that the pulse counter records one count in a T_c sec slot time is then given by

$$p = \lambda_n P_d + (1 - \lambda_n) P_f$$

and the probability of no counts is equal to $1 - p$. In a 1-sec observation interval there are $n = 1/T_c = 10^8$ T_c-sec slots. Thus, under a Poisson assumption on the dark current photoelectron emission statistics, the number of pulse counter counts in a 1-sec observation period is a binomial (n, p) random variable.

Suppose now that the threshold γ is set at 200 μV, σ = 34 μV and $\overline{G} = 10^6$. Then the receiver operating curve gives P_d = 0.91 and $P_f = 2 \times 10^{-9}$. Under these conditions $np \cong n\lambda_n P_d = 23$ when $n = 10^8 >> 1$. In this case the binomial (n, p) distribution is approximately Poisson with intensity np, so the number of recorded pulse counter counts will still be Poisson even with the random photomultiplier gain and the amplifier thermal noise taken into account. Next, suppose the threshold γ is set lower at 100 μV. Here the receiver operating curve gives P_d = 0.962 and $P_f = 2 \times 10^{-3}$. In this case $np \cong nP_f = 2 \times 10^5 >> 1$ when $n = 10^8$ and the binomial (n, p) distribution is approximately Gaussian with mean np and variance $np\,(1 - p)$. The pulse counter data will no longer be Poisson. Therefore, care must be taken in using pulse counter data for determining counting statistics. Specifically, if the counter threshold is set too low, the photocathode emission false alarm rate will be too high and the counter statistics will be dominated by the thermal (Gaussian) noise of the PMT preamp.

C. Noise and Signal Pulse Detection: Receiver Operating Curves

Whereas phase I of this demonstration was concerned with the dark current statistics of the PMT, in phase II the laser is added to evaluate the error performance of the PMT-preamplifier combination in detecting the presence of laser light excitation. In this demonstration phase, the laser is either on or off in a time slot of duration T_s seconds. The PMT amplifier output is integrated over this time period, normalized by T_s and compared to a threshold γ. Detection of the laser light is declared if and only if the threshold is exceeded. In Ref. 10, the error performance of this detector was evaluated assuming that photocathode emission events are Poisson distributed and taking into account the random gain density (1) as well as the preamplifier thermal noise. Specifically, consider the detector shown in Fig. 5, where the amplifier is assumed to introduce an additive white Gaussian noise $V(t)$ with spectral density N_0 given by (3) to the signal $S(t)$ across the anode resistor R. Let

$$P_{ds} = \text{probability of correctly detecting the presence of incident laser light} \tag{6}$$

and

$$P_{dn} = \text{probability of correctly detecting the absence of incident laser light} \tag{7}$$

These detection probabilities P_{ds} and P_{dn} depend on the thermal noise level N_0, the threshold γ, the integration time T_s, and the average gain $\overline{G}$ and dark current of the PMT, as well as the incident light intensity at the photocathode. Specifically let

$$\overline{N}_n = \text{average number of dark current photocathode emissions per } T_s \text{ sec time period at the photocathode} \tag{8}$$

and

$$\overline{N}_s = \text{average number of light-excited photocathode emission events per } T_s \text{ sec time period}$$

$$= \frac{\eta P_s}{hf}, \tag{9}$$

where η is the photocathode quantum efficiency, P_S is the incident signal light intensity at the photocathode surface, h is Planck's constant and f the incident light center frequency. Also define

$$\sigma_1^2 = N_0/T_s$$

and let

$$P(\alpha) = e^{\alpha\left(e^{-\overline{G}/B} - 1\right)} Q\left(\frac{\gamma}{\sigma_1}\right)$$

$$+ \frac{\sqrt{\overline{G}}}{B} e^{-\alpha} \sum_{n=0}^{\infty} \frac{\sqrt{n}\left(\alpha e^{-\overline{G}/B}\right)^n}{n!} J_n \qquad (10)$$

where

$$J_n = \int_0^{\infty} Q\left(\frac{\gamma - \left(\frac{eR}{T_s}\right)y}{\sigma_1}\right) \frac{e^{-y/B}}{\sqrt{y}} I_1\left(2\frac{\sqrt{n\overline{G}y}}{B}\right) dy$$

and B is given by (2). It was shown in Ref. 10 that

$$P_{ds} = P(\alpha)\Big|_{\alpha = \overline{N}_s + \overline{N}_n}, \qquad (11)$$

and

$$1 - P_{dn} = P(\alpha)\Big|_{\alpha = \overline{N}_n} \qquad (12)$$

Typical on-off pulse detection receiver operating curves of P_{ds} versus $1 - P_{dn}$ are shown in Fig. 6 for integration time $T_s = 100$ ns, thermal noise standard deviation $\sigma_1 = 34\ \mu$V and for several values of $\overline{N}_s$. Figure 6(a) shows the results for $\overline{G} = 10^6$ and 25 dark current counts/second. Figure 6(b) shows the corresponding results for $\overline{G} = 3.2 \times 10^6$ and 53 dark current counts/sec[1].

[1]The PMT average gain can be increased by increasing the relative anode voltage. Gains from 10^5 to 10^7 can be produced in this way. However, increasing the anode voltage results in an increase in the number of dark current electrons drawn from the photocathode. The values of dark current used in Fig. 6 correspond to the RCA 31034 PMT operating at -30°C at the various values of gain (see Fig. 12 of Section IV).

D. Uncoded PPM Performance

Phase III of the demonstration involves the addition of pulse position modulation and demodulation equipment to the optical and elementary electronic signal detection equipment. In M-ary PPM signaling M adjacent time slots, each of duration T_s sec, are used to form a single PPM symbol. A given T_s second slot is either a "noise slot," in which case no light is emitted from the laser diode transmitter, or a "signal slot" when light of a constant intensity is emitted from the laser. In a PPM symbol time one, and only one, of the slots is a signal slot and the remaining $(M - 1)$ slots are noise slots. Since the information to be transmitted is contained in the position (in time) of the signal slot, each PPM symbol can convey $\log_2 M$ bits of information (if perfectly detected). In the 2.5-bit/detected photon demonstration $M = 256$, but we shall perform the analysis for arbitrary M.

The PPM demodulator receives signal slot/noise slot decisions over the slot time T_s from the PMT and light detector circuit of Fig. 5. Since separate decisions are provided to the demodulator for each of the M slots in a PPM symbol, a number of different types of error events are possible. We will analyze each of these event statistics below.

1. PPM symbol erasure probability. When no signal slot decisions are received during an entire PPM symbol a symbol erasure is declared. The probability of this event, P_E, is the probability that the signal slot is not detected and that the remaining $(M - 1)$ noise slots are correctly classified. In the notation of Fig. 6,

$$P_E = (1 - P_{ds}) P_{dn}^{M-1} \qquad (13)$$

which can be easily evaluated given an operating point on that figure.

2. Undetected PPM symbol error probability. An undetected symbol error occurs when the signal slot is incorrectly declared a noise slot and one (and only one) of the noise slots is taken as a signal slot. Since the incorrectly detected noise slot can occur at any one of $(M - 1)$ places, the probability, P_{us}, of an undetected symbol error is

$$P_{us} = (M - 1)(1 - P_{ds})(1 - P_{dn}) P_{dn}^{M-2} \qquad (14)$$

3. Correct PPM symbol detection probability. When a PPM symbol is transmitted it will be received correctly if the signal slot and all of the noise lots are correctly detected. The probability of this event is

$$P_c = P_{ds} P_{dn}^{M-1} \qquad (15)$$

4. **Two or more pulse probability.** When two or more pulses are received during a PPM symbol time the demodulator has conflicting instructions. The probability of this event, P_{2P} is easily derived as follows:

$$P_{2P} = Pr(\text{no pulses detected}) - Pr(1 \text{ pulse detected})$$

$$= 1 - P_E - P_c - P_{us}$$

$$= 1 - P_{dn}^{M-1} - (M-1)(1-P_{ds})(1-P_{dn})P_{dn}^{M-2}. \quad (16)$$

5. **Uncoded PPM symbol error probability.** The above events are all measurable during the phase III tests and are important in determining the overall performance of the system when coding is later applied. However, it is also possible to consider the system as purely an uncoded PPM system during phase III. If this is to be accomplished then some resolution of erasures and multiple pulses per symbol time must be accomplished. A maximum likelihood demodulator would use the following decision rules:

(1) If all M slots are declared noise slots, choose the transmitted signal slot at random from the M slots.

(2) If exactly $k \geq 1$ slots are declared signal slots, choose the transmitted signal slot at random from among those k slots.

The actual PPM demodulator does not use these rules. Whenever an erasure occurs it always selects a preassigned symbol as its output. Also, if two or more pulses are received in a symbol time, the output symbol corresponds to the first detected signal slot. However, since the transmitted PPM symbols are selected at random and the channel is assumed to be memoryless, the performance of the actual decoder will be the same as the maximum likelihood version. We will therefore analyze the latter.

Since the demodulator always produces an output symbol then the probability of a symbol error, P_S, is 1 minus the probability of correct symbol detection. (Note that the correct symbol probability is *not* P_c as developed above. This is because P_c assumes that neither erasures nor multiple pulses are resolved. P_c is therefore only one component in the uncoded PPM probability of correct symbol detection.) We have, therefore, that

$$P_S = 1 - P_r(\text{correct symbol detection})$$

$$= 1 - P_{ds}(P_{dn})^{M-1} - \frac{1}{M}(1-P_{ds})P_{dn}^{M-1}$$

$$- \sum_{k=1}^{M-1} \frac{1}{k+1}\binom{M-1}{k} P_{dn}^{M-1-k}(1-P_{dn})^k P_{ds} \quad (17)$$

where the second term corresponds to P_c, the third term is the probability of correct decision when an erasure occurs and the last term corresponds to the probability of a correct symbol selection when the actual signal slot and one or more noise slots are declared signal slots. In the appendix it is shown that (17) simplifies to

$$P_S = 1 - \frac{1}{M}(1-P_{ds})P_{dn}^{M-1} - \frac{P_{ds}\left(1-P_{dn}^{M}\right)}{M(1-P_{dn})} \quad (18)$$

6. **Uncoded PPM bit error probability.** The final quantity of interest is the probability of a bit error for the uncoded PPM configuration. Since PPM is a form of orthogonal modulation, the bit error probability P_b and the PPM symbol error probability can be related by

$$P_b = \left(\frac{\frac{M}{2}}{M-1}\right) P_S \quad (19)$$

During the phase III evaluation P_b will be one of the key performance parameters. Figure 7 shows P_b as a function of the information power efficiency measure $\rho = \log_2 M/\overline{N}_S$ (bits/photon) for several values of the analog detector threshold γ, $M = 256$, $\sigma = 34$ μV and $T_s = 100$ ns. Figure 7a shows the result for $\overline{G} = 10^6$ and 25 dark current counts/second whereas Fig. 7b is for $\overline{G} = 3.2 \times 10^6$ and 53 counts/second. In both figures the performance improves as the threshold γ is reduced from 250 to 150 μV. This is because the pulse erasure probability is also decreasing. However, if the threshold is reduced too far, the noise generated false alarm rate increases, which in turn increases P_b. This effect is evident in the $\gamma = 100$ μV curves. Nevertheless, even with an optimization of the threshold it is clear that without the benefits of the overall coding system, operation at a reasonable error rate is not possible at 2.5 bits/photon.

E. Coded PPM Performance

In the final demonstration phase, a Reed-Solomon (R-S) encoder and decoder are used over the PPM modulated channel. Since the code symbol alphabet size is 8 bits (matched to the PPM symbol size), the (R-S) code blocklength, N, is $2^8 - 1 = 255$ (symbols) (Ref. 11). Two specific codes were considered for the demonstration. The first is the (255,223), $t = 16$ error correcting, rate 7/8 (approx.) code. The second is the (255,191), $t = 32$ error correcting code which has a rate of approximately 3/4.

A t error correcting (R-S) code can correct any combination of t or less symbol errors. It can also compensate for combinations of errors and erasures. In particular, if s is the number of decoder input symbol errors and e is the number of decoder input symbol erasures, then the decoder will produce the correct output codeword provided

$$2s + e < d_{min} \triangleq 2t + 1 \tag{20}$$

The code is therefore more powerful at correcting erasures than errors.

One can easily show that if the confidence that a particular decoder input symbol is correct is strictly less than 0.5, it is better to erase the symbol and allow the decoder to attempt to fill it in. This condition is always satisfied whenever a PPM erasure occurs *or* whenever two or more pulses are received in a PPM symbol time. (The case of two pulses can also result when the signal slot is not detected and two noise slots are declared signal slots.) Thus, when (R-S) coding is used, it is necessary to modify the demodulator decision rules. Toward this end let us define a decoder input symbol error event to be the occurrence of an undetected PPM symbol error, and a decoder input symbol erasure as either a PPM symbol erasure or the occurrence of two or more pulses in a PPM symbol time. Then, from Eqs. (13 – 16), the probabilities of decoder input symbol error $P_{\mathscr{S}}$ and symbol erasure $P_{\mathscr{E}}$ are given by

$$P_{\mathscr{S}} = P_{us} = (M-1)(1-P_{ds})(1-P_{dn})P_{dn}^{M-2} \tag{21}$$

and

$$P_{\mathscr{E}} = P_E + P_{2P} = 1 - P_{ds}P_{dn}^{M-1} - (M-1)(1-P_{ds})(1-P_{dn})P_{dn}^{M-2} = 1 - P_c - P_{us}. \tag{22}$$

Once we have $P_{\mathscr{S}}$ and $P_{\mathscr{E}}$ we can compute the decoder output performance. A (R-S) decoder will always produce the correct codeword at the output whenever the error/erasure capability of the code (Eq. 20) is satisfied. When this condition is not satisfied the decoder finds that it cannot solve the equations which determine the location of the codeword symbol errors nor can it solve for the values of the erased symbols. Consequently, a decoding (computational) failure results. The codes considered are systematic, which means that each codeword is made up of 255-2t encoder input information symbols followed by 2t generalized parity symbols (which are computed in the encoder). When a decoding failure occurs, the decoder will output the systematic portion of the codeword. This means that for that particular codeword the power of the code is not (actually cannot be) used, but the uncoded portion of the codeword is still more likely to be correct than a randomly selected codeword.

The probability that the incorrect codeword is selected by the decoder, P_{WE}, can be written by inspection as

$$P_{WE} = \sum_{s=0}^{N} \sum_{e=\Delta}^{N-s} \binom{N}{s} \binom{N-s}{e} P_{\mathscr{S}}^{s} P_{\mathscr{E}}^{e} (1 - P_{\mathscr{S}} - P_{\mathscr{E}})^{N-s-e} \tag{23}$$

where

$$\Delta = max\,(d_{min} - 2s, 0).$$

The argument of the summation in (23) is recognized as the probability that a received codeword contains s symbol errors, e erasures and the remaining N-s-e symbols are error- and erasure-free. The summation is then taken over all values of s and e which violate Eq. (20). The symbol = is used since (23) is actually a slight overbound. This is because there is some chance (albeit extremely small) that, even though (20) is violated, the systematic portion of the codeword is received without error.

The probability of a decoder output symbol error P_{SE} can now be computed by assuming that when s and e errors and erasures respectively occur in a codeword, they are statistically spread uniformly over the N codeword symbols. Then assuming that all symbol erasures are (pessimistically) resolved in error at the decoder output gives

$$P_{SE} = \sum_{s=0}^{N} \sum_{e=\Delta}^{N-s} \binom{N}{s} \binom{N-s}{e} \cdot P_{\mathscr{S}}^{s} P_{\mathscr{E}}^{e} (1 - P_{\mathscr{S}} - P_{\mathscr{E}})^{N-s-e} \left(\frac{s+e}{N}\right) \tag{24}$$

Given P_{SE} we can also compute P_{BE}, the decoder output bit error rate from the expression

$$P_{BE} = \frac{M}{2(M-1)} P_{SE}. \tag{25}$$

Equation (25) is the final performance measure for the 2.5-bit/detected photon demonstration. Figure 8 shows P_{BE} as a function of the energy efficiency parameter ρ for a PMT gain

of 3.2×10^6, 53 dark counts/second, $T_s = 100$ ns and several values of pulse detector threshold voltage γ. Figure 8(a) illustrates the performance of the rate 7/8 code whereas Fig. 8(b) applies to the rate 3/4 code. It is clear from these figures that the rate 7/8 code will not produce an adequate bit error rate at $\rho = 2.5$ bits/photon. The rate 3/4 code, on the other hand, provides Voyager threshold performance up to 2.9 bits/photon for $\gamma = 150$ μV.

The corresponding performance curves for a PMT gain of 10^6 were not computed since it was recognized that they would not provide adequate performance. This can be seen from the following analysis. From Fig. 7(a) we see that the uncoded PPM bit error rate at $\rho = 2.5$ bits/photon and a PMT gain of 10^6 is greater than 0.15 for all values of γ. From (19) this corresponds to a PPM symbol error rate of 0.3, which results from undetected symbol errors and incorrectly resolved ambiguities. This implies that on the average a (R-S) codeword of length 255 will have 76 anomalies, either symbol errors or erasures. Since this number exceeds the code correction capabilities (Eq. 20) of both codes *even if all anomalies are erasures*, the coded performance will obviously be inadequate. Contrast this with the 3.2×10^6 gain results of Fig. 7(b). At $\rho = 2.5$ and $\gamma = 150$ μV the average number of anomalies per codeword is 20. This satisfies Eq. (20) for the rate 7/8 code only if most are erasures. For the rate 3/4 code, however, (20) is satisfied on the average regardless of whether the anomalies are erasures or errors.

One additional comment is in order. The demonstration goal is to achieve 2.5-bit/detected photon performance *at 100 kbps*. The performance calculations in this section were made for $T_s = 100$ ns, which corresponds to the maximum clock rate of the logic used in the hardware. For 256-ary PPM and rate 3/4 coding, these results correspond to 234 kbps.

IV. Experimental Results of Phase I

A. Experimental Setup and Conditions

As described earlier, the purpose of this phase of the work was to measure the intrinsic noise characteristics of the system and to verify the theory used to model it.

The block diagram of the experimental setup is shown in Fig. 9. The photomultiplier tube (PMT) used in the experiment was the RCA model C31034. This PMT has a GaAs photocathode with the highest quantum efficiency available at the wavelength region where AlGaAs lasers operate (0.8-0.9 μm). This particular PMT type has a quantum efficiency (η) of about 15% at 0.85 μm. A selected type of this PMT – Model C31034A-02 – with $\eta \cong 20\%$ was also purchased but was not used in the experiment. The above efficiency values are at room temperature, and a moderate improvement is obtained with some cooling. The typical gain of this PMT is 10^6. The gain varies with varying experimental conditions, as will be described below.

Since the dark current of the PMT is too high at room temperature, the PMT was placed in a cooled housing. The cooling reduces the thermionic emission from the PMT's photocathode, which is a dominant noise mechanism. The thermoelectric (T.E.) cooler used was a Model TE-206TS-RF (Products for Research, Inc.), which can cool the photocathode to a temperature 60 K lower than room temperature. Due to other noise mechanisms (Ref. 12), some temperature-independent residual dark current was observed below about -30°C. The high voltage (1200-1800V) is supplied to the PMT by a Model 204-10 power supply (Pacific Photometric Instruments).

The output of the PMT was directly connected to a fast preamplifier Model 9301 (ORTEC). This amplifier has a gain of 10, bandwidth of 150 MHz and equivalent input noise voltage of about 34 μV rms.

The PMT and preamplifier (which must be in close proximity because of noise considerations) were placed in a dark enclosure to eliminate ambient illumination and permit the observation of the actual PMT and preamp noise mechanisms. The effectiveness of the enclosure was verified by noting that no change in the dark count reading resulted when the laboratory was darkened or fully illuminated. Following the preamplifier was a second amplifier (HP Model 461) which provided final pulse gain (gain: X100, bandwidth: 150 MHz).

The amplified signal was first fed to a fast storage oscilloscope (Tektronix 7834) to verify that the PMT noise output was generated by single photocathode emission events, not bursts of events (Ref. 13). In all subsequent tests the amplified signal was connected to a HP5370A universal counter, which in turn was connected to a HP9845C computing controller through an HP-IB interface.

In the course of the measurements there were basically three parameters that could be changed: The temperature of the photocathode, the PMT voltage and the threshold (or trigger) level of the counter. Changing the temperature alters the intensity of the noise process, i.e., the number of photoelectrons released from the photocathode via thermionic emission (Ref. 14). Changing the PMT voltage V changes the average gain $\bar{G}$ of the PMT according to

$$\bar{G} = aV^b$$

where V is in kilovolts, $\overline{G}$ is in units of 10^6 and where $a \approx 0.043$ and $b \approx 9.22$ are constants calculated from the manufacturer's data sheet. Finally, changing the threshold level changes both the intensity of the dark current counts and their origin. At low threshold voltages most of the counts are due to white (Gaussian) thermal noise of the preamplifier; at higher values of threshold voltages the dominant noise mechanism is due to the dark counts originating at the PMT.

Several limitations on the measurements are imposed due to hardware constraints. First, the bandwidth of the preamplifier-amplifier combination is slightly less than 110 MHz; this matches the 100-MHz capability of the counter, but is somewhat less than the 140-MHz intrinsic bandwidth of the PMT. Secondly, when the counter operates in the time interval mode (as needed for the time-of-arrival distribution measurement), it counts only every other interval and, in addition, has a 330-μs deadtime after each measurement. This limitation is not significant if we assume that the process is stationary and when operating in the Poisson regime, but for low values of threshold voltage, only the frequency mode of the counter can be used in order to obtain reliable results.

B. Experimental Results

The first experiment set was designed to test the validity of the assumption that the dark count events are generated by a Poisson process. To eliminate counts due to preamplifier thermal noise the counter threshold voltage was set at the 9σ level of the thermal process. A sample set of 1000 count events was then observed and compared in two ways against theoretical predictions. The first comparison involved the computation of the number of events in a preset time interval to verify that it was Poisson distributed. The second involved computation of the event interarrival times to determine if they were exponentially distributed. Typical experimental results are shown in Fig. 10 along with the associated theoretical distributions. Figure 10(a) shows the frequency distribution (variation in the number of counts per time interval), whereas Fig. 10(b) contains the interarrival time distributions. The results show extremely good agreement between theory and experiment. Additionally, two χ-square tests appropriate for the comparisons of these distributions were computed. These tests confirmed the visual conclusions that the theoretical and experimental distributions were close. Similar results were obtained for several different values of PMT gains.

Measurements were also made at lower values of the counter threshold voltage. Here, as expected, the measured distributions deviated considerably from the Poisson model due to the increased number of counts resulting from preamplifier thermal noise.

The second experiment set involved taking extensive data to determine the average intensity of the dark current Poisson process, as well as its variation with system parameters. First, the dependence of the dark current intensity on PMT temperature was measured and compared with the manufacturer's specifications. Favorable agreement was obtained which provided confidence that the experimental setup was performing correctly. Then, the effects of PMT gain and counter threshold voltage on the dark current intensity were measured. To obtain reliable results, 10^4 seconds of data were collected for each gain and threshold setting. The results are shown in Fig. 11. As expected, the average intensity of noise events decreases with an increase in the counter threshold voltage.

Another important feature of Fig. 11 is the rather large dependence of the dark current intensity on the PMT gain setting. This phenomenon is due to the fact that as the voltage of each dynode is increased, the PMT enters an unstable region produced by regenerative ionization effects (Ref. 12). It is important that this variation be adequately modeled so that optimized systems designs can be obtained. However, the data of Fig. 11 includes not only the effects of the PMT but the preamplifier and counter threshold as well. By modeling the overall process and working backward from the experimental results one can deduce the intrinsic variation in PMT dark current intensity as a function of PMT gain. This result is shown in Fig. 12. The figure clearly indicates an exponential dark current dependence on average gain.

V. Conclusions

We have described the 2.5-bit/detected photon demonstration program and identified how it has been broken into four demonstration phases. Then an analysis of each phase was presented. The analysis illustrated how, with 256-ary PPM modulation, Reed-Solomon coding and carefully chosen system parameters, it is possible to achieve the 2.5-bit/detected photon goal at rates above 100 kbps. Finally, the results of the phase I experiments were presented where the agreement between theory and experiment was shown to be surprisingly close. Additionally, the parametric dependencies of the PMT detection noise intensities were also experimentally determined.

The agreement in the phase I tests provides a substantial amount of credibility to the analysis and associated conclusions presented herein. However, the final proof will come with the actual phase IV demonstration. Nevertheless, the results of phase I will permit the phase II-IV activities to be conducted with increased optimism.

Acknowledgment

The authors wish to express their appreciation to Gary Lorden for his assistance on the statistical data analysis algorithms used in Phase I.

References

1. Katz, J., and Lesh, J. R., "Optical Communications for Deep Space Missions Using Integrated Semiconductor Injection Lasers," Jet Propulsion Laboratory, Pasadena, Calif., (in preparation).
2. Katz, J., "High Power Semiconductor Lasers for Deep Space Communications," in *The TDA Progress Report 42-63*, pp. 40-50, Jet Propulsion Laboratory, Pasadena, Calif., June 15, 1981.
3. Pierce, J. R., "Optical Channels: Practical Limits with Photon Counting," *IEEE Trans. Comm.*, Vol. COM-26, No. 12, pp. 1819-1821, Dec. 1978.
4. Gordon, J. P., "Quantum Effects in Communications Systems," Proceedings of the Institute of Radio Engineers," Vol. 50, pp. 1898-1908, Sept. 1962.
5. Levitin, L. B., "Photon Channels with Small Occupation Numbers," *Problemy Predachi Informatsii*, Vol. 2, No. 2, pp. 60-68, 1966.
6. Helstrom, C. W., Liu, J. W. S., and Gordon, J. P., "Quantum Mechanical Communication Theory," *Proc. IEEE*, Vol. 58, pp. 1578-1598, Oct. 1970.
7. Helstrom, C. W., "Capacity of the Pure State Quantum Channel," *Proc. IEEE*, Vol. 62, pp. 140-141, Jan. 1974.
8. McEliece, R. J., "Practical Codes for Photon Communication," *IEEE Trans. Information Th.*, Vol. IT-27, 1981.
9. Massey, J. L., "Capacity, Cutoff Rate, and Coding for a Direct Detection Optical Channel," in *TDA Progress Report 42-60*, pp. 68-76, Jet Propulsion Laboratory, Pasadena, Calif., Dec. 1981.
10. Tan, H. H., "A Statistical Model of the Photomultiplier Gain Process with Applications to Optical Pulse Detection," Jet Propulsion Laboratory, Pasadena, Calif., (in preparation).
11. McEliece, R. J., *The Theory of Information and Coding*, Addison-Wesley, Reading, MA, 1977.
12. Engstrom, R. W., "Photomultiplier Handbook," Ch. 4, RCA Solid-State Div., Lancaster, PA 17604, 1980.
13. McHose, R. E., "Time Characteristics of Photomultipliers – some General Observations," RCA application note AN-4884, 1972.
14. Katz, J., "The Deep Space Optical Channel: I. Noise Mechanisms," *TDA Progress Report 42-64*, pp. 180-186, Jet Propulsion Laboratory, Pasadena, Calif., Aug. 15, 1981.

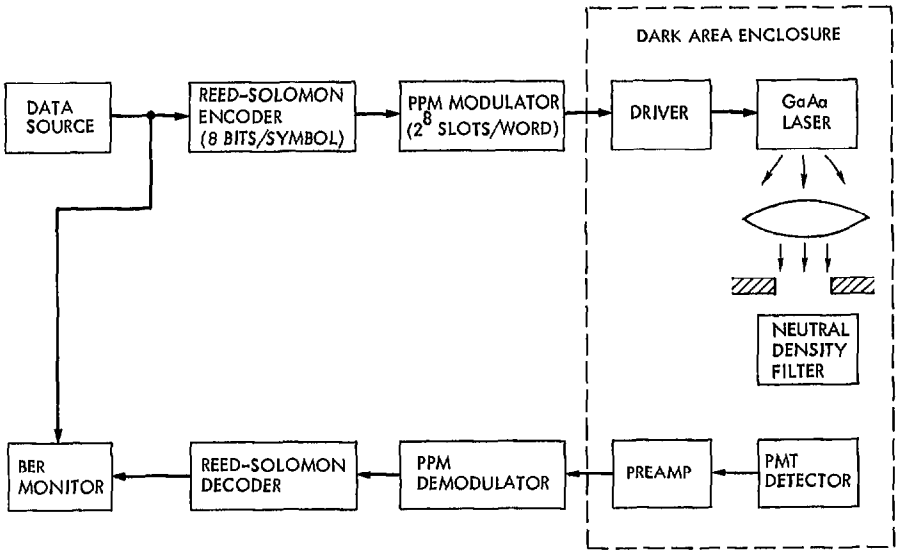

Fig. 1. Block diagram of 2.5-bit/detected photon demonstration system

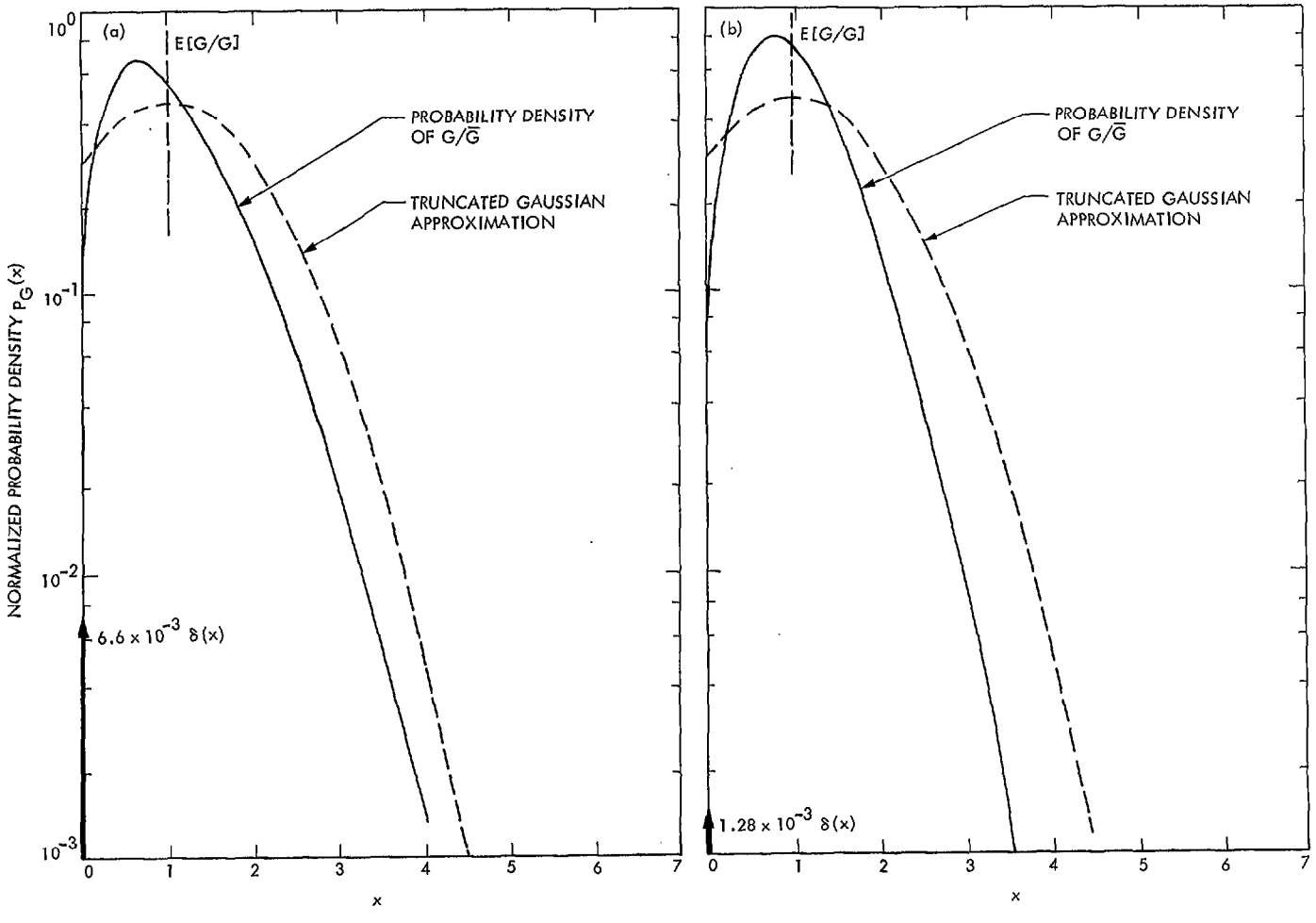

Fig. 2. Probability density function of the normalized gain of an eleven-stage PMT and (a) average gain = 10^6, (b) average gain = 10^7

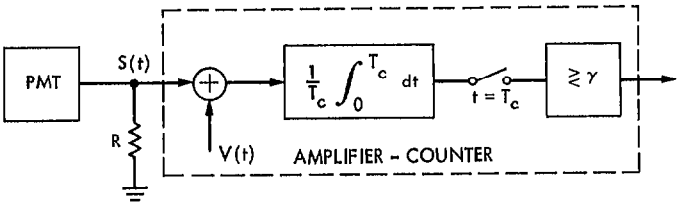

Fig. 3. Equivalent block diagram of the PMT noise model measurement system

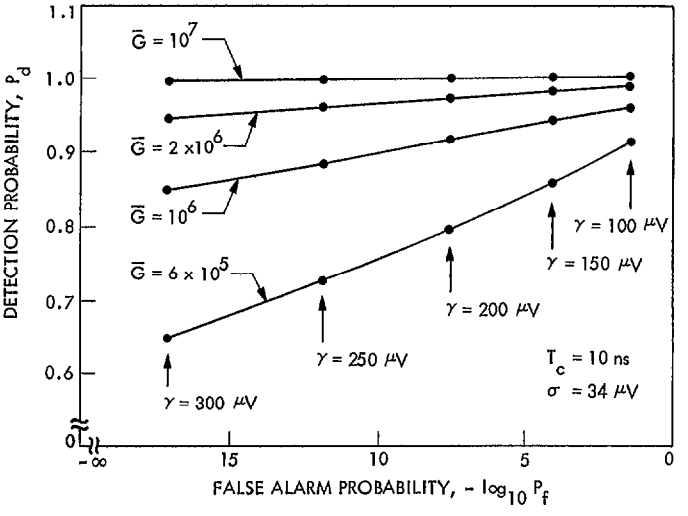

Fig. 4. Detection and false alarm probabilities (conditioned on a photocathode emission event)

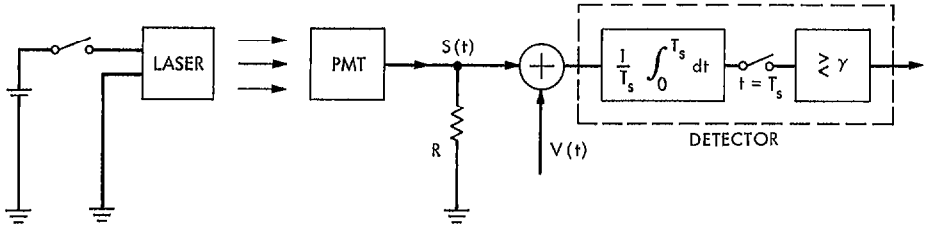

Fig. 5. Equivalent block diagram of phase II demonstration

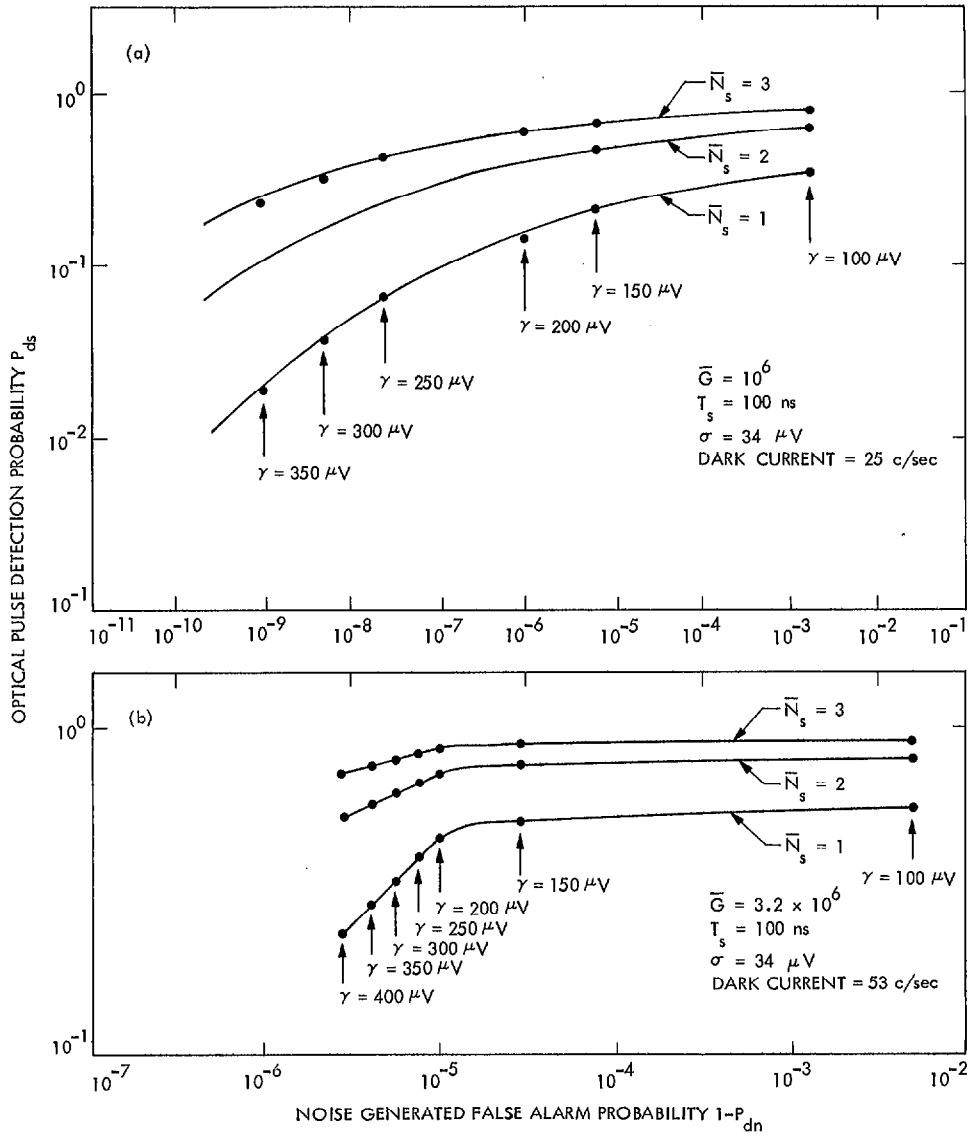

Fig. 6. Optical pulse detection and false alarm probabilities for $\bar{N}_s$ photoelectrons emitted per pulse: (a) PMT gain = 10^6, 25 dark counts/sec, (b) PMT gain = 3.2×10^6, 53 dark counts/sec

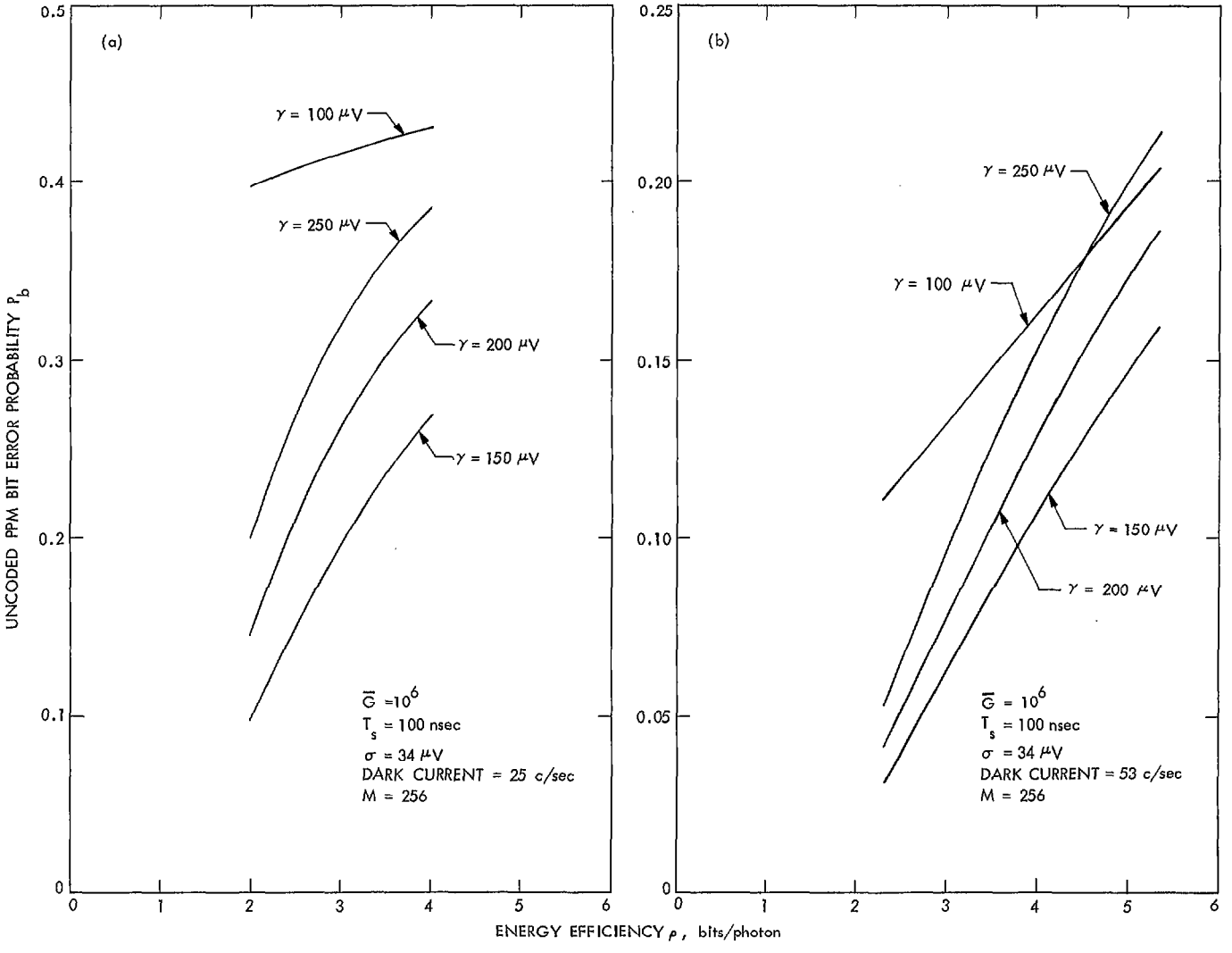

Fig. 7. Bit error performance for uncoded 256-ary PPM: (a) PMT gain = 10^6, 25 dark counts/sec, (b) PMT gain = 3.2×10^6, 53 dark counts/sec

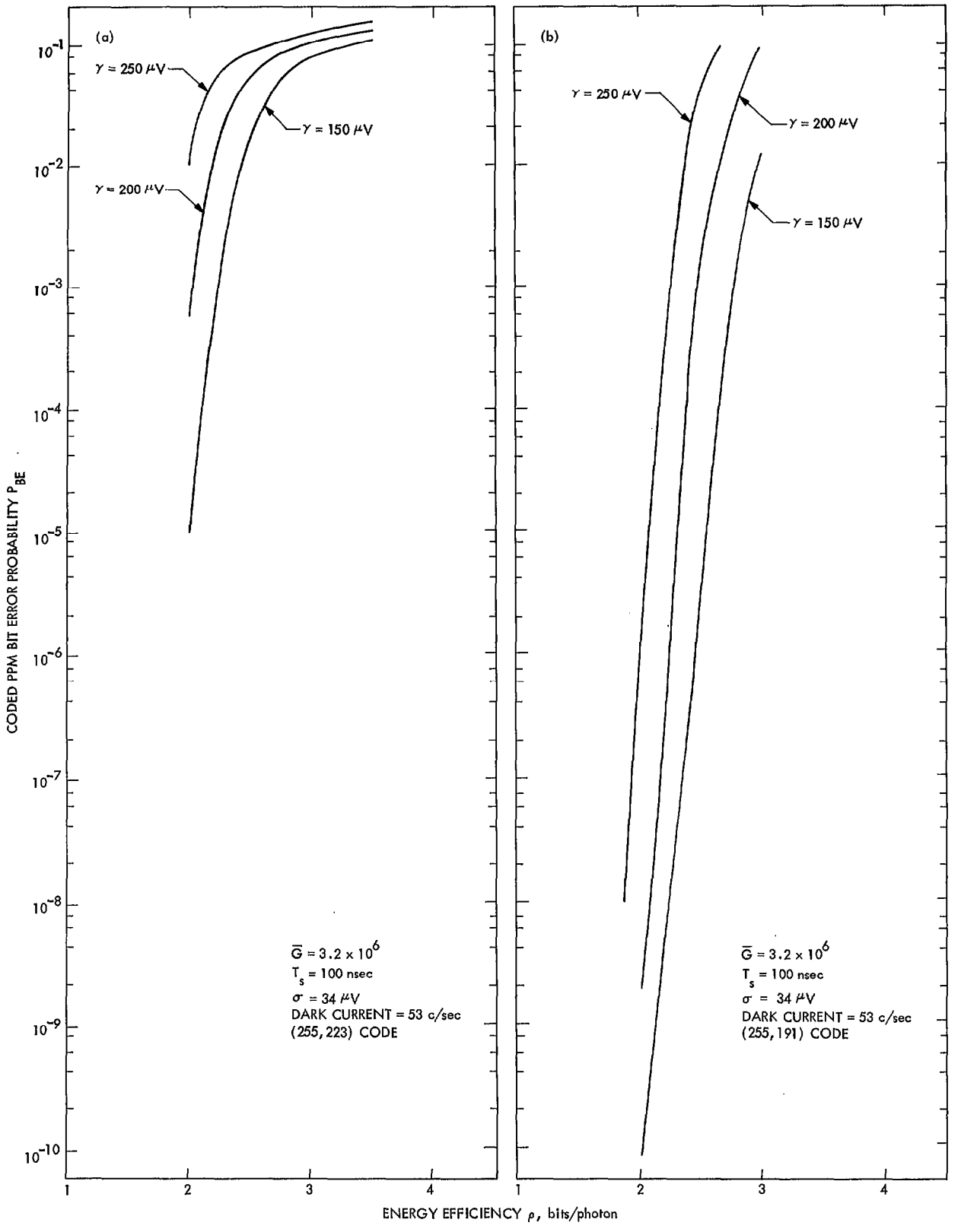

Fig. 8. Coded bit error performance for PMT gain of 3.2×10^6 and 53 dark counts/second: (a) (255,223) rate 7/8 R-S code, (b) (255,191) rate 3/4 R-S code

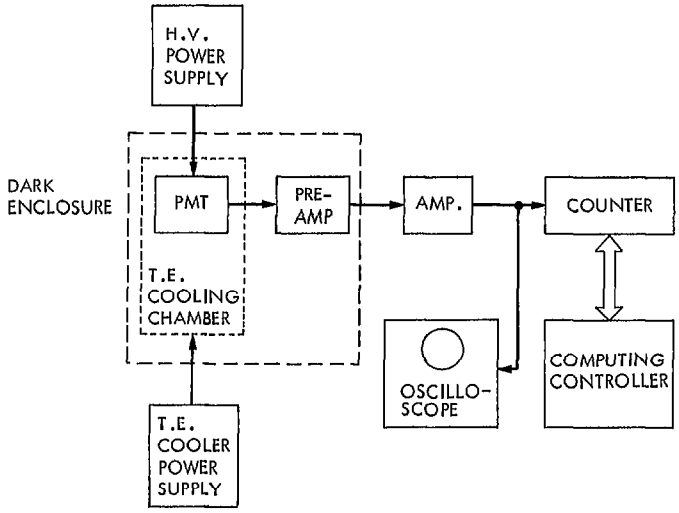

Fig. 9. Experimental setup for phase I test

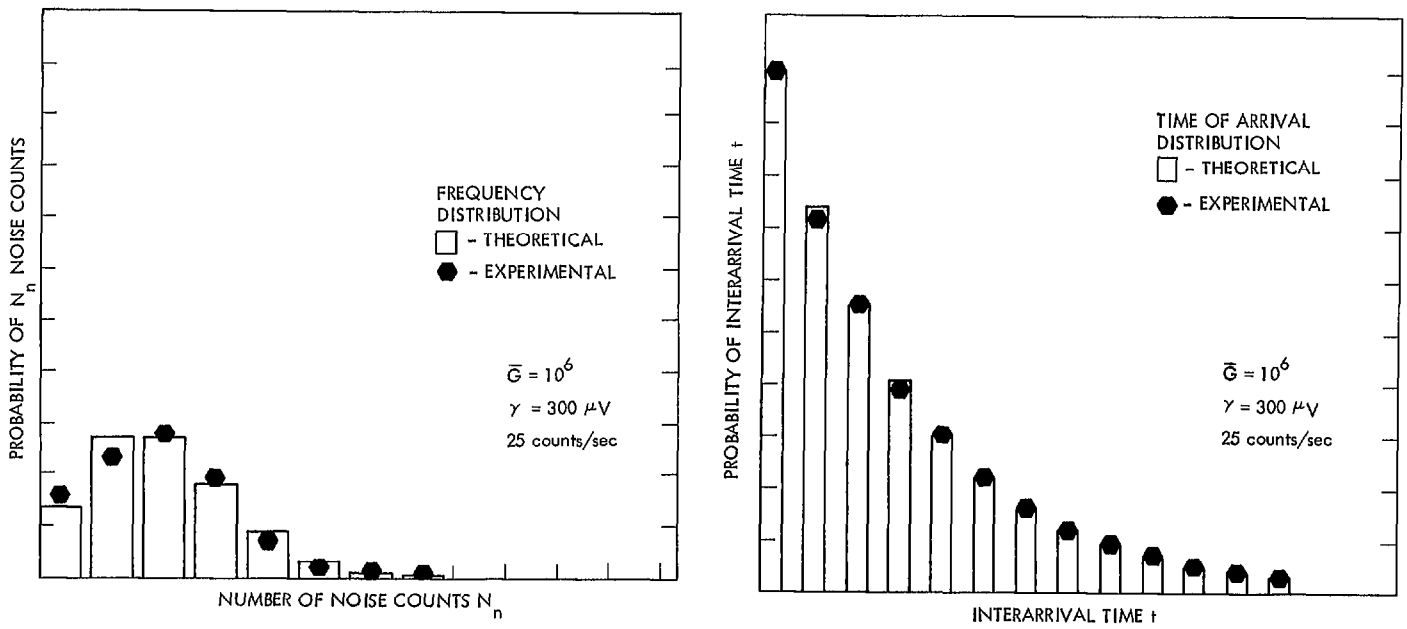

Fig. 10. Theoretical and experimental dark count noise distributions (gain = 10^6, 25 dark counts/sec): (a) frequency distribution (theory = Poisson), (b) interarrival time distribution (theory = exponential)

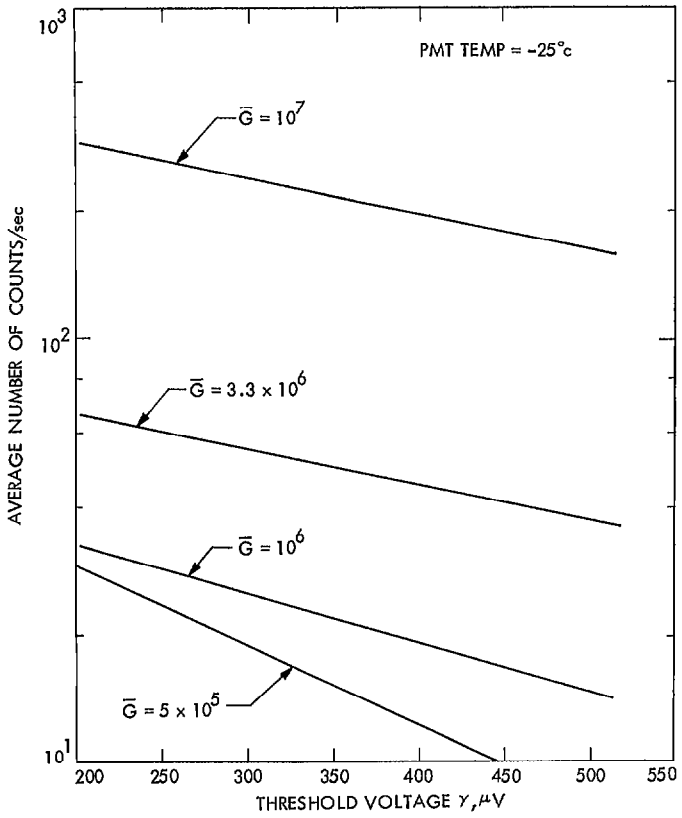

Fig. 11. Measured PMT - amplifier dark current intensity

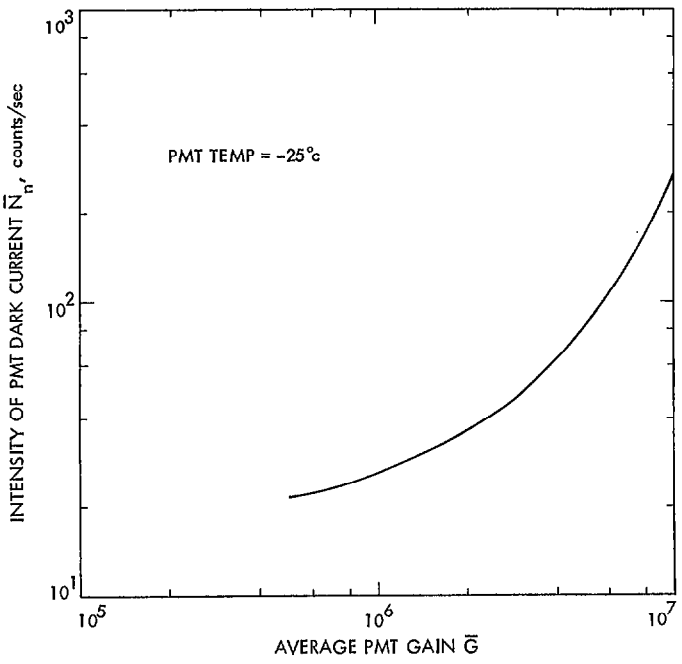

Fig. 12. Variation in PMT dark current intensity with average PMT gain

Appendix

In Section III we found that the uncoded PPM symbol error probability was given by (Eq. 17)

$$P_S = 1 - P_{ds}(P_{dn})^{M-1} - \frac{1}{M}(1 - P_{ds})P_{dn}^{M-1}$$

$$- \sum_{k=1}^{M-1} \frac{1}{k+1}\binom{M-1}{k} P_{dn}^{M-1-k}(1 - P_{dn})^k P_{ds} \quad \text{(A-1)}$$

Combining the second and fourth terms and changing the index of summation yields

$$P_S = 1 - \frac{1}{M}(1 - P_{ds})P_{dn}^{M-1}$$

$$- \sum_{k=1}^{M} \frac{1}{k}\binom{M-1}{k-1} P_{dn}^{M-k}(1 - P_{dn})^{k-1} P_{ds}$$

Then multiplying and dividing the last term by $M(1 - P_{dn})$ produces

$$P_S = 1 - \frac{1}{M}(1 - P_{ds})P_{dn}^{M-1}$$

$$- \frac{P_{ds}}{M(1 - P_{dn})} \sum_{k=1}^{M} \binom{M}{k} P_{dn}^{M-k}(1 - P_{dn}^k)$$

$$= 1 - \frac{1}{M}(1 - P_{ds})P_{dn}^{M-1} - \frac{P_{ds}(1 - P_{dn}^M)}{M(1 - P_{dn})} \quad \text{(A-2)}$$

which is the desired result.

That this expression is correct can be seen from the following analysis.[2] The second term is clearly the probability of making a correct symbol decision when a PPM symbol erasure occurs (cf Eq. 13). The last term of equation (A-2) must therefore be the probability of correct decision when one or more pulses occur in the PPM symbol. Let us hypothesize a different demodulator decision rule. We will assume that erasures are still resolved by the roll of an M-sided die, but that in the event of one or more pulses in a symbol time, the first pulse is *always* taken as correct. This demodulation rule is really equivalent to the maximum-likelihood decision rule when the inputs to the demodulator are equally likely and one is interested in average probability of error. (Note: the actual demodulator uses a modified form of this rule.) For this new demodulator the probability of correct symbol decision given that the actual signal slot was the first slot is P_{ds}. The probability of correct decision given the second slot was actually sent is likewise $P_{dn}P_{ds}$. Continuing on in this manner and using the fact that each of the conditions has equal chance of occurring results in

$$P_r \text{ (correct decision and one or more pulse received)}$$

$$= \frac{1}{M}(P_{ds} + P_{dn}P_{ds} + P_{dn}^2 P_{ds} + \cdots + P_{ds}^{M-1}P_{ds})$$

This clearly equals the last term of Eq. (A-2).

[2]The authors are indebted to R. Stokey for this interpretation.